Inorganic Chemistry

Article

pubs.acs.org/IC

Rational Design of a Cytotoxic Dinuclear Cu_2 Complex That Binds by Molecular Recognition at Two Neighboring Phosphates of the DNA Backbone

Thomas Jany,[†] Alexander Moreth,[‡] Claudia Gruschka,[†] Andy Sischka,[§] Andre Spiering,[§] Mareike Dieding,[§] Ying Wang,[§] Susan Haji Samo,[§] Anja Stammler,[†] Hartmut Bögge,[†] Gabriele Fischer von Mollard,[‡] Dario Anselmetti,[§] and Thorsten Glaser*[,†]

[†]Lehrstuhl für Anorganische Chemie I, Chemistry Department, [‡]Lehrstuhl für Biochemie III, Chemistry Department, and [§]Experimentelle Biophysik, Physics Department, Bielefeld University, Universitätsstrasse 25, 33615 Bielefeld, Germany

Supporting Information

ABSTRACT: The mechanism of the cytotoxic function of cisplatin and related anticancer drugs is based on their binding to the nucleobases of DNA. The development of new classes of anticancer drugs requires establishing other binding modes. Therefore, we performed a rational design for complexes that target two neighboring phosphates of the DNA backbone by molecular recognition resulting in a family of dinuclear complexes based on 2,7-disubstituted 1,8-naphthalenediol. This rigid backbone preorganizes the two metal ions for molecular recognition at the distance of two neighboring phosphates in DNA of 6−7 Å. Additionally, bulky chelating pendant arms in the 2,7-position impede nucleobase complexation by steric hindrance. We successfully synthesized the Cu^{II}_2 complex of the designed family of dinuclear complexes and studied its binding to dsDNA by independent ensemble and single-molecule methods like gel electrophoresis, precipitation, and titration experiments followed by UV−vis spectroscopy, atomic force microscopy (AFM), as well as optical tweezers (OT) and magnetic tweezers (MT) DNA stretching. The observed irreversible binding of our dinuclear Cu^{II}_2 complex to dsDNA leads to a blocking of DNA synthesis as studied by polymerase chain reactions and cytotoxicity for human cancer cells.

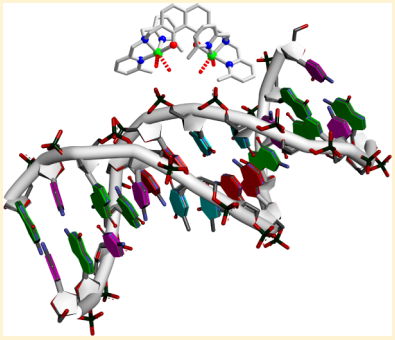

INTRODUCTION

Nucleic acids are polymers from condensation of phosphoric acid with alcohol groups of ribose (RNA) or desoxyribose (DNA) that possess heterocyclic purine and pyrimidine bases as side chains.[1] Thus, these polyphosphodiesters offer several potential binding sites for metal ions. Each phosphate group contributes one negative charge to the overall charge of the polymer that is electrostatically balanced by a layer of alkali metal and Mg^{II} ions. On the other hand, transition metal ions often bind specifically by coordination to nucleobases and phosphates, while coordination to the sugar moieties is rare.[2] Another way metal complexes can bind to the nucleobases of DNA is by intercalation of a planar aromatic functionality between the base pairs of double-helical DNA.[3] The glycopeptide antibiotic bleomycine is a prominent example for an interaction of a metal complex with nucleic acids, which offers therapeutical applications.[4] A prominent example for binding to the nucleobases is the major anticancer drug cisplatin (*cis*-$[PtCl_2(NH_3)_2]$). Upon cellular uptake, cisplatin binds to DNA preferentially via a 1,2-intrastrand binding d(GpG) at N7 of purine bases with guanine is favored over adenine,[5,6] resulting in a strong bending of the DNA.[6,7] This interferes with the molecular recognition of essential proteins for transcription, as RNA polymerases,[8,9] which is supposed to cause the cytotoxicity of cisplatin. As a single drug or in combination with other drugs, cisplatin is used in the treatment for testicular, bladder, ovarian, head and neck, cervical, and lung cancers.[8,10] The application of cisplatin is limited by acquired resistance to cisplatin[11] and by severe side effects in normal tissues. In particular, nephrotoxicity is a major factor that limits the use and efficiency of cisplatin in cancer therapy.[12] To overcome the limitations of cisplatin and to broaden the range of treatable tumors, a lot of efforts have been devoted to improve cisplatin.[13] Many analogs of cisplatin have been synthesized resulting in second-generation cisplatin drugs like oxaliplatin and carboplatin.[14]

In addition to the binding at the nucleobases, the phosphates of the DNA backbone are known to be the target of the metal active sites of enzymes such as nucleases. These metalloenzymes catalyze the hydrolytic cleavage of the phosphoester bonds that are thermodynamically unstable toward hydrolysis but kinetically highly inert.[15,16] The active sites consist of one or more metal ions that provide several pathways to accelerate hydrolysis as Lewis-acid activation, leaving group stabilization or providing a metal-bound hydroxide as nucleophile. This reactivity usually implies the formation of a metal−phosphate oxygen bond during the catalytic cycle. However, this bond

Received: November 28, 2014
Published: February 4, 2015

DOI: 10.1021/ic5028465
Inorg. Chem. 2015, 54, 2679−2690

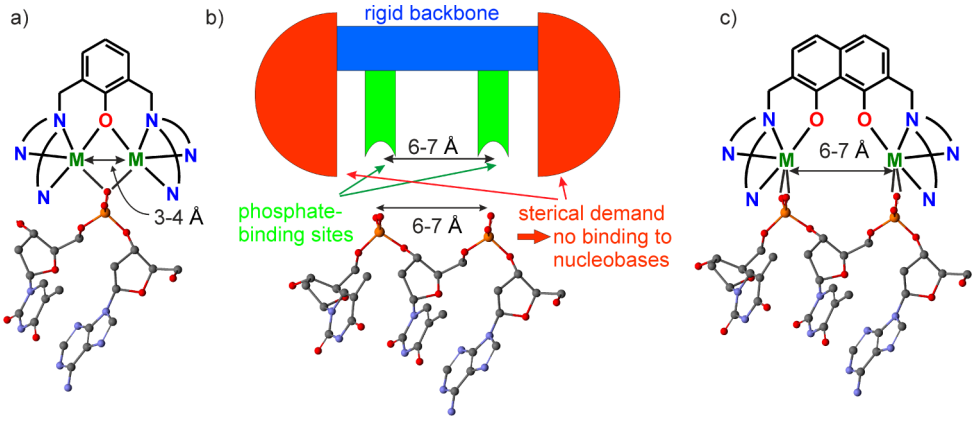

Figure 1. (a) Family of dinuclear complexes with hydrolytic reactivity based on dinucleating Robson ligands with a central phenolate. Two metal ions coordinate to one DNA phosphate. (b) Design concept for a dinuclear complex binding to two neighboring phosphates of the DNA backbone. (c) Molecular realization by a family of dinuclear complexes based on 2,7-disubstituted 1,8-naphthalenediol ligands. Please note that the two metal ions cannot coordinate to one DNA phosphate but are preorganized to coordinate to two neighboring DNA phosphates.

must be labile enough to be cleaved in the catalytic cycle to enable product release. This reactivity has stimulated intense research to mimic structure and function of the active sites of these nucleases and closely related phosphatases by biomimetic model complexes.[17] A prominent family of dinuclear model complexes (e.g., with Cu^{II}) that not only mimic the hydrolytic cleaving reactivity of nucleases but also of peptidases has been synthesized using phenol-based, dinucleating Robson ligands with pendant chelating arms in the 2,6-position (Figure 1a).[16,18,19] A main mode of action is a bridging coordination of one phosphate to both metal ions (Lewis-acid activation) facilitated by a metal−metal distance of 3−4 Å with one metal ion providing a bound hydroxide as nucleophile.

There has been recent success in the field by increasing the level of complexity to incorporate details of the second coordination sphere in the active sites.[20] These developments include the combination of a hydrolytically active metal site with DNA binding groups such as amine and guanidine groups for hydrogen bonding, positively charged residues for electrostatic interactions, or minor-groove binding motives.[21]

However, the hydrolytic cleavage of the bound phosphoester destroys the DNA−metal complex that foils the formation of a stable metalated DNA adduct. Therefore, a metal complex as efficient binder to DNA phosphates must provide a strong thermodynamic and kinetic driving force with low hydrolytic activity. Herein, we report on the rational design of a dinuclear complex family that is supposed to bind to two neighboring phosphates of the DNA backbone by molecular recognition without having an unwanted hydrolytic activity. We demonstrate the irreversible binding ability of the dinuclear Cu^{II}_2 complex to DNA by several independent biochemical, spectroscopic, and single-molecule methods. Furthermore, we show that this compound inhibits DNA synthesis and is cytotoxic to human cancer cells at the same concentration, which provides evidence that DNA binding causes the inhibition of DNA synthesis that leads to the death of the cancer cells.

EXPERIMENTAL SECTION

General Considerations. Solvents and starting materials were of the highest commercially available purity and used as received. All reactions were carried out under an argon atmosphere. The synthesis of MOM_2**1** was described previously.[22] Bis((6-methylpyridin-2-yl)methyl)amine has been synthesized according to a modified literature procedure.[23] Infrared spectra (400−4000 cm^{-1}) of solid samples were recorded on a Shimadzu FTIR-8300 or a Shimadzu FTIR 8400S spectrometer as KBr disks. ESI and MALDI-TOF mass spectra were recorded on a Bruker Esquire 3000 ion trap mass spectrometer and a PE Biosystems Voyager DE mass spectrometer, respectively. For acquisition of high-resolution mass spectra a Bruker APEX III FT-ICR has been used. ^1H and ^{13}C NMR spectra were recorded on a Bruker Avance 600 spectrometer using the solvent as an internal standard. The assignments of the NMR resonances were supported by 2D HMBC and HMQC spectroscopy. Elemental analyses were carried out on a LECO CHN-932 or a HEKAtech Euro EA elemental analyzer. UV−vis−NIR absorption spectra of solutions were measured on a Shimadzu UV-3101PC spectrophotometer in the range 190−3200 nm at ambient temperatures. Temperature-dependent magnetic susceptibilities were measured by using a SQUID magnetometer (MPMS XL-7 EC, Quantum Design) in a static field of 1 T in the range 2−290 K. For calculations of the molar magnetic susceptibilities, χ_m, the measured susceptibilities were corrected for the underlying diamagnetism of the sample holder and the sample by using tabulated Pascal's constants. The JulX program package was used for spin-Hamiltonian simulations and fitting of the data by a full-matrix diagonalization approach.[24]

Synthesis of 2,7-Bis(*N*,*N*-di((6-methylpyridin-2-yl)methyl)-aminomethyl)-1,8-bis(methoxymethoxy)naphthalene (MOM_2tom^{Me}). Solid $Na[BH(OAc)_3]$ (1.11 g, 5.25 mmol) is added to a solution of 2,7-diformyl-1,8-bis(methoxymethoxy)naphthalene (MOM_2**1**) (532 mg, 1.75 mmol) and di((6-methylpyridin-2-yl)-methyl)amine (DPA^{Me}) (795 mg, 3.50 mmol) in 1,2-dichloroethane (70 mL). The resulting suspension is stirred for 18 h at room temperature and then for 4 h at 50 °C. The reaction is quenched by addition of NH_4OH solution (1 M, 350 mL). The aqueous layer is extracted with CH_2Cl_2 (6 × 70 mL), and the organic extracts are combined, dried over Na_2SO_4, and concentrated in vacuo, resulting in a yellow oil of high viscosity. The crude product is purified by column chromatography (basic aluminum oxide, THF). Yield: 1.01 g (1.39 mmol, 79%). ^1H NMR (600 MHz, $CDCl_3$): δ/ppm =7.73 (d, J = 8.5 Hz, 2 H, H10), 7.52 (t, J = 7.7 Hz, 4 H, H4), 7.56 (d, J = 8.5 Hz, 2 H, H11), 7.45 (d, J = 8.5 Hz, 4 H, H5), 6. 96 (d, J = 7.7 Hz, 4 H, H3), 4.94 (s, 4 H, H15), 3.98 (s, 4 H, H8), 3.83 (s, 8 H, H7), 3.48 (s, 6 H, H16), 2.49 (s, 12 H, H1). ^{13}C NMR (125 MHz, $CDCl_3$): δ/ppm = 159.6 (C2), 157.5 (C6), 150.1 (C14), 136.6 (C4), 136.2 (C12), 130.1 (C9), 127.4 (C10), 124.8 (C11), 121.4 (C3), 121.2 (C13), 119.5 (C5), 101.2 (C15), 60.5 (C7), 58.0 (C16), 52.6 (C8), 24.5 (C1). HR-ESI-MS ($CHCl_3$/MeOH m/z): calcd for $[M + H]^+$ $C_{44}H_{51}N_6O_4$ 727.39663, found 727.39477; calcd for $[M + Na]^+$ $C_{44}H_{50}N_6O_4Na$ 749.37858, found 749.37649. UV−vis (CH_3CN): $\tilde{\nu}$/cm^{-1} (ε/10^3 M^{-1} cm^{-1}): 42 400 (73.5), 37 500 (25.1), 30 260 (1.79). IR (KBr): $\tilde{\nu}$/cm^{-1} = 3441 s, 3416 s, 3059 w, 3007 w, 2922 m, 2852 w, 2824 w, 1591 s,

DOI: 10.1021/ic5028465
Inorg. Chem. 2015, 54, 2679−2690

1577 s, 1474 s, 1433 s, 1358 m, 1329 m, 1157 s, 1020 s, 955 s, 926 s, 788 s.

Chart 1

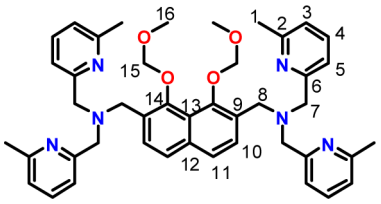

Synthesis of [(tom^{Me}){Cu(OAc)}$_2$] ($Cu_2(OAc)_2$). A solution of MOM_2tom^{Me} (370 mg, 0.509 mmol) in MeOH (35 mL) is added dropwise to a solution of copper acetate ($Cu(OAc)_2 \cdot H_2O$) (208 mg, 1.04 mmol) in MeOH (35 mL). The greenish-blue solution is stirred for 25 h at 40 °C, resulting in a color change to a greenish-black. The solvent is removed under vacuum. Upon slow diffusion of Et_2O into a solution of the residue in CH_3CN/H_2O (14:1), blue crystals were obtained. Yield: 314 mg (0.300 mmol, 60%). ESI-MS (MeOH, m/z): 382.1 $[M - 2OAc]^{2+}$, 881.2 $[M + H]^+$. IR (KBr): $\tilde{\nu}/cm^{-1}$ = 3397 m br, 3067 w, 3055 w, 3011 w, 3011 w, 2970 w, 2926 w, 2859 w, 1611 s, 1584 s, 1530 m, 1472 m, 1449 m, 1395 s, 1375 s, 1341 m, 1288 w, 1271 w, 1254 w, 1219 w, 1200 w, 1165 w, 1142 w, 1099 w, 1078 w, 1055 m, 1022 w, 1001 w, 968 w, 876 w, 831 m, 787 m, 679 m, 648 w, 621 w, 586 w, 567 w, 523 w, 502 w, 469 w. UV-/Vis (CH_3CN): $\tilde{\nu}/cm^{-1}$ (10^3 ε/M^{-1} cm^{-1}): 42 100 sh (45.1), 27 900 (9.9), 23 900 (0.54), 18 500 (0.34), 14 800 (0.34). Anal. Calcd for $C_{44}H_{63}N_6Cu_2O_{14.5}$ [(tom^{Me}){Cu(OAc)}$_2$]·8.5 H_2O): C, 51.06; H, 6.14; N, 8.12. Found: C, 51.14; H, 6.03; N, 7.74

Single-Crystal X-ray Diffraction. A crystal of [(tom^{Me}){Cu(OAc)}$_2$]·9.75H_2O·CH_3CN was measured at 100(2) K on a Bruker Kappa APEXII diffractometer (four-circle goniometer with 4K CCD detector, Mo Kα radiation, focusing graphite monochromator). Crystal and refinement data: M = 1098.66 g mol^{-1}, $C_{46}H_{68.50}Cu_2N_7O_{15.75}$, orthorhombic, space group $P2_12_12_1$, a = 10.9107(16) Å, b = 15.793(2) Å, c = 31.758(5) Å, V = 5472.3(14) Å^3, Z = 4, ρ = 1.334 g/cm^3, μ = 0.847 mm^{-1}, F (000) = 2310, crystal size = 0.37 × 0.23 × 0.14 mm^3, 57 003 reflections ($3.43 < \Theta < 27.00°$) collected, 11 883 reflections unique. Absolute structure parameter = −0.003 (10), R = 0.0436 for 10 494 reflections with $I > 2\ \sigma(I)$, R = 0.0521 for all reflections. Crystallographic data are deposited at the Cambridge Crystallographic Data Centre as supplementary publication no. 936123 ($Cu_2(OAc)_2$). These data can be obtained free of charge from the Cambridge Crystallographic Data Centre via www.ccdc.cam.ac.uk/data_request/cif.

Atomic Force Microscopy. λ-DNA (400 pM λ-DNA equivalent to 40 μM DNA bases/phosphates) was incubated with 50 and 200 μM $Cu_2(OAc)_2$ for 15 min at room temperature in TRIS buffer (150 mM KCl, 10 mM Tris/HCl, pH 8.0) as well as in double-distilled ultrapure water (18.2 MΩcm). A 10 μL amount of the solution was incubated for 15 min on freshly cleaved mica, subsequently rinsed by ultrapure water (18.2 MΩcm), and carefully dried in a nitrogen steam. AFM measurements were performed with a commercial instrument (Nanoscope V, Multimode, Bruker) at room temperature under ambient conditions in tapping mode of operation using single-crystal Si-cantilevers (Bruker).

DNA Overstretching with Optical Tweezers. Streptavidin-coated polystyrene microspheres (Spherotech, IL) with a diameter of 3.05 μm (0.5% w/v) were diluted 1:1000 in 150 mM NaCl, 10 mM Tris/HCl at pH 8.0 and introduced into the sample chamber.[25] One bead was trapped with the optical tweezers,[26] handed over to the glass micropipette, and held tightly by applying low pressure. A second bead was then trapped remaining inside the optical trap. λ-DNA was biochemically functionalized[27] on both ends with several biotins to ensure tethering to the beads. The functionalized λ-DNA (15 pM in 150 mM NaCl, 10 mM Tris/HCl at pH 8.0) was then introduced into the sample chamber to allow immobilization between the two beads.[27] Then a first λ-DNA overstretching experiment was done with a velocity of 1 μm/s to an end-to-end distance of ∼18 μm and immediately relaxed. Comparison with the literature-based dsDNA reference elasticity curve (transitional/melting plateau at ∼64 pN) ensured that only one single DNA molecule is bound between the microbeads. This force/extension curve serves as a reference. In a second step, a solution of 6 μM $Cu_2(OAc)_2$ in 150 mM NaCl, 10 mM Tris/HCl at pH 8.0 was added into the sample chamber. After a typical waiting time of at least 2 min, where $Cu_2(OAc)_2$ is supposed to bind to the DNA strand, subsequent DNA overstretching experiments were performed. All experiments were conducted at 20 °C.

DNA Torsional Stretching with Magnetic Tweezers. We used a commercial magnetic tweezers instrument (Picotwist, Lyon, France) where the magnetic bead position is determined by an optical microscopic setup with a CCD camera. 4.2 μm short double-stranded DNA fragments were functionalized with multibiotins at one end and multidigoxigenins at the other end for magnetic tweezers (MT) experiments. These DNA fragments were immobilized via several antidigoxigenins at the bottom cell wall and via their biotins on streptavidin-coated paramagnetic beads (MyOne, Dynabeads, Life-Technologies). All MT experiments were conducted in adapted PBS buffer (137 mM NaCl, 27 mM KCl, at pH 7.4; 0.1% BSA, 0.1% TWEEN 20). Typical incubations times were 30 (digoxigenin) and 15 min (biotin). The multiple surface binding ensures a torsionally constraint immobilization of the DNA fragment which is of crucial importance for the experiment. Successful multivalency binding and a nick-free DNA can be confirmed by optically inspecting the rotation of the DNA-bead complex via external magnetic field rotation. A proper preparation induces DNA plectonemic superspiralization and shortening of the DNA. All MT experiments were conducted at 25 °C.

Plasmid Binding of $Cu_2(OAc)_2$ and Analysis by Agarose Gel Electrophoresis. pBluescript SK$^+$ plasmid DNA (2960 base pairs, bp) was isolated from *E. coli* strain XL1 blue. A 1.25 μg amount of plasmid DNA (100 μM DNA bases/phosphates) was incubated in 20 mM HEPES pH = 7.5 without addition, with $Cu_2(OAc)_2$, copper chloride ($CuCl_2 \cdot 2H_2O$), or MOM_2tom^{Me} for 1 h at 37 °C. To obtain corresponding concentrations of copper ions the molar concentration of copper chloride was 2-fold higher than that of $Cu_2(OAc)_2$. The DNA was separated by agarose gel electrophoresis in TBE buffer (89 mM Tris base, 89 mM boric acid, 2 mM EDTA), stained with ethidium bromide, and viewed under UV light. Digital pictures were quantified to determine the fraction of supercoiled, open-circular, and linear plasmid DNA. Cleavage of a single phosphodiester bond in a supercoiled plasmid induces relaxation into the open-circular form. A plasmid is linearized by cleavage of both strands in close proximity, for example, by the restriction enzyme *Eco*RI.

Quantification of DNA Binding of $Cu_2(OAc)_2$. A 20 μg amount of pBluescript SK$^+$ plasmid DNA (600 μM DNA bases/phosphates) was incubated in 20 mM HEPES pH 7.5 without addition or with 100 μM to 3 mM $Cu_2(OAc)_2$ for 1 h at 37 °C in a total volume of 100 μL. DNA was precipitated by addition of $NaClO_4$ to 75 mM and ethanol to 70% final concentration for 3 days at −20 °C.[28] DNA was pelleted by centrifugation for 20 min with 13 000 rpm in a microcentrifuge, rinsed with 70% ethanol, and resuspended in 100 μL of 20 mM HEPES pH 7.5. Absorption at 356 nm was determined in a UV−vis spectrometer to calculate the concentration of Cu_2^{2+}. The DNA precipitation efficiency was determined from samples without $Cu_2(OAc)_2$ by absorption at 260 nm and used for correction of the binding data.

PCR. A 380 bp insert was amplified from the plasmid pBK38 encoding mouse vti1b using the oligonucleotide primer GGAATTCATGGCCGCCTCCGCCGC and CGGGATCCTATTGAGACTGTAGTCGATTC.[29] About 2.3 ng of plasmid DNA (0.34 μM DNA bases/phosphates), 0.1 μM primer (together 5.3 μM DNA bases/phosphates), 250 μM dNTPs, and various concentrations of metal complexes were used per reaction. Taq DNA polymerase was used for DNA amplification. After 17 PCR cycles the reaction products were analyzed by agarose gel electrophoresis.

Survival of HeLa Cells. Two thousand five hundred HeLa cells were plated in 96-well plates in DMEM medium with 5% FCS and

DOI: 10.1021/ic5028465
Inorg. Chem. 2015, 54, 2679−2690

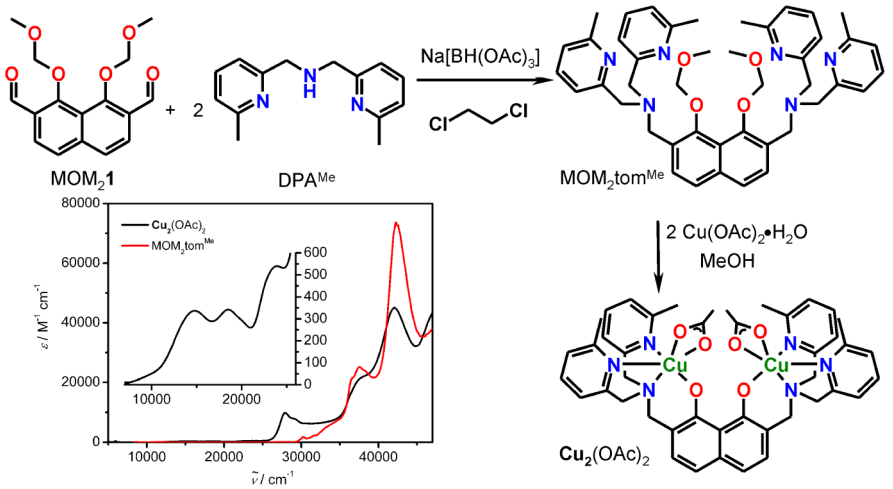

Figure 2. Synthesis of the targeted complex $\mathbf{Cu_2}(OAc)_2$. (Inset) Electronic absorption spectra of $\mathbf{Cu_2}(OAc)_2$ and MOM_2tom^{Me} measured in CH_3CN solutions at ambient temperatures.

incubated for 24 h at 37 °C 5% CO_2. The cells were further incubated for 3 days without addition or with the indicated concentrations of metal complexes in triplicates. Cells were inspected with a microscope. Cell survival was assayed with sulforhodamine B according to published procedures.[30] Briefly, cells were fixed with trichloroacetic acid and stained with 0.4% sulforhodamine B in 1% acetic acid. Cells were washed and dried. Bound sulforhodamine B was solubilized with 10 mM Tris base and the absorption at 564 nm determined in an ELISA plate reader. Sulforhodamine B binds to proteins and therefore is an established way to measure cell proliferation and survival. Averages of 3 wells for each condition were calculated in three independent experiments and compared to untreated controls set as 100% survival. Similar results were obtained by testing cell survival with the XTT assay, which measures metabolic reduction of a tetrazolium reagent to a formazan.

RESULTS AND DISCUSSION

Rational Design of a Complex Family Binding Neighboring Phosphates of DNA. Inspired (i) by the cytotoxicity of cisplatin due to its strong binding to the nucleobases of DNA and (ii) by the hydrolytic cleaving ability of transition metal ions of nucleases and their model complexes due to coordination to the phosphates of DNA we designed a new lead motif that binds by molecular recognition to the phosphate backbone of DNA and not to the nucleobases. The freedom in the choice of the metal ion allows controlling the reactivity of these complexes to exhibit either hydrolytic activity or a strong binding affinity to DNA without hydrolytic activity.

In order to achieve coordination of a metal complex to the phosphates of the DNA backbone the complex and ligand design must on one hand involve a source of molecular recognition for the phosphate groups and on the other hand impede complexation with the nucleobases that are located in the minor and major groove and thus less exposed. We are following the multivalence principle, which states that several preorganized binding sites connected by a rigid backbone are not only enthalpically but also entropically favored as only the first binding event costs loss of degrees of freedom.[31] In this respect, our concept relies on the molecular recognition of two neighboring phosphodiester groups by a dinuclear metal complex, in which a rigid ligand backbone predefines the metal−metal distance to ∼6−7 Å, the distance of two neighboring phosphates in the DNA backbone (Figure 1b). Furthermore, the coordination environment must provide some sterical hindrance to prevent a potential competing binding to the less exposed nucleobases. Inspired by the success of the complexes of phenol-based Robson ligands (Figure 1a), whose metal−metal distances of 3−4 Å preorganize the metal ions to bind both to the same phosphate,[16,18,19] we came up with the idea to create an extended ligand system based on 1,8-naphthalenediol that would be able to enforce metal−metal distances of 6−7 Å with sterically demanding pendant arms in the 2,7-position (Figure 1c). Furthermore, this rigid backbone prohibits coordination of both metal ions to the same phosphate. It should be noted that a dinuclear Cu^{II} complex, whose ligand compartments are connected by a flexible 1,8-naphthalene spacer, was reported recently,[32] but a binding of both Cu^{II} ions to one phosphate has been proposed due to the strong flexibility. Variation of the metal ions (divalent vs trivalent, 3d vs 4d vs 5d) may allow a fine tuning of the kinetic and thermodynamic stability so that potentially a new family of DNA-binding molecules evolves that can be cytotoxic to cancer cells. The variation of the binding mode in comparison to cisplatin-based drugs may provide access to the treatment of different cancer types with different toxicity.

Herein, we present the synthesis of the first complex of this new family with Cu^{II} ions. The kinetically labile Cu^{II} ion has a thermodynamic driving force for DNA complexation. Binding constants of Cu^{II} complexes that catalyze the hydrolytic cleavage of DNA have been reported in the order of 10^3−10^4.[33] Although Cu^{II} complexes of tridentate ligands are active in hydrolytic cleavage of phosphoesters, those of tetradentate ligands are less active. This reactivity difference may be related to the Jahn−Teller effect that usually results in a tetragonal elongated coordination environment for Cu^{II} complexes. A tridentate ligand provides two coordination sites: one for phosphate binding (Lewis-acid activation) and one for hydroxide binding (providing the reactive nucleophile). On the other hand, a tetradentate ligand provides only one coordination site of significant binding energy (not in the Jahn−Teller axis) open either for phosphate binding or for hydroxide binding resulting in the reduced hydrolytic reactivity. Furthermore, it has been proposed that endogenous metals like copper may be equally effective but less toxic than platinum complexes.[34]

Synthesis and Characterization. We already established a streamlined synthesis of 2,7-diformyl-1,8-naphthalenediol

DOI: 10.1021/ic5028465
Inorg. Chem. 2015, 54, 2679−2690

(H_2**1**)[22] and applied it for the preparation of a trinucleating ligand via Schiff-base condensation with 2 equiv of *N*,*N*-dimethylethylenediamine.[35] It should be noted that analogous ligands have recently been used for the preparation of efficient olefine polymerization catalysts.[36] Initially, we attempted a reductive amination of the free diol H_2**1** with DPA^{Me}, which was not successful. However, the reductive amination of the MOM-protected precursor MOM_2**1** with DPA^{Me} using Na[$BH(OAc)_3$] afforded the protected ligand MOM_2tom^{Me} (Figure 2).

While MOM-protecting groups are easy to cleave with Brønsted acids, this route proved to be not applicable for MOM_2tom^{Me} due to the six basic nitrogen atoms, which underwent protonation followed by precipitation before cleavage. We thus thought that a metal ion that is already coordinated in the N_3 ligand compartment of MOM_2**1** could act as a Lewis acid for MOM deprotection as it has been observed for thioethers.[37] In this respect, reaction of MOM_2**1** with copper acetate at 40 °C resulted in the clean MOM deprotection, and the targeted complex [(tom^{Me}){Cu($OAc)_2$}$_2$] (= **Cu$_2$**($OAc)_2$) has been isolated (Figure 2). Complex formation can be monitored by UV−vis spectroscopy, as a prominent aryloxide → Cu^{II} LMCT transition at 27 900 cm^{-1} appears for the deprotected complex accompanied by d−d transitions in the range 14 000−25 000 cm^{-1} (Figure 2 inset).

The molecular structure of **Cu$_2$**($OAc)_2$ has been established by single-crystal X-ray diffraction and is shown in different orientations in Figure 3. A thermal ellipsoid plot is provided in

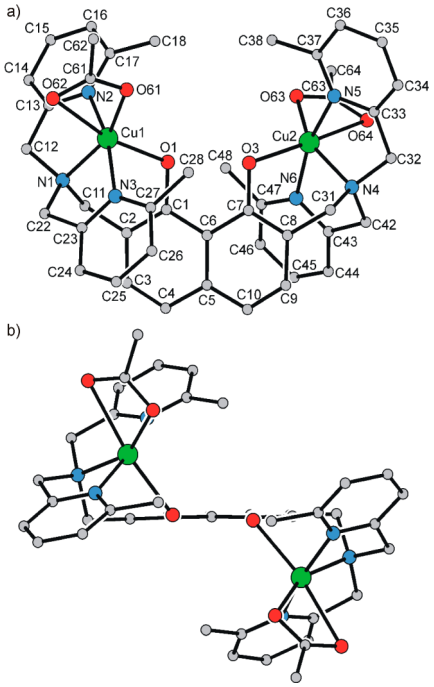

Figure 3. Molecular structure of **Cu$_2$**($OAc)_2$ in crystals of **Cu$_2$**($OAc)_2$·9.75H_2O·CH_3CN in two different orientations (a and b) and labeling scheme used (b). Hydrogen atoms are omitted for clarity.

Figure S1, Supporting Information, and selected interatomic distances and angles are summerized in Table 1. Two Cu^{II} ions are coordinated in the N_3O compartments of the deprotected ligand (tom^{Me})$^{2-}$. The octahedral coordination environments are saturated by bidentate OAc^- ligands. One oxygen donor of the acetate (Cu−O = 2.58 and 2.55 Å) and the aryloxides of the

Table 1. Selected Interatomic Distances (Angstroms) and Angles (degrees) for $Cu_2(OAc)_2$·9.75H_2O·CH_3CN

Cu1−O1	2.284(2)	O62−Cu1−N1	99.07(10)
Cu1−O61	1.968(2)	O62−Cu1−N2	90.60(10)
Cu1−O62	2.580(3)	O62−Cu1−N3	92.16(10)
Cu1−N1	2.015(3)	N1−Cu1−N2	82.41(12)
Cu1−N2	2.043(3)	N1−Cu1−N3	82.34(11)
Cu1−N3	2.057(3)	N2−Cu1−N3	164.75(12)
Cu2−O3	2.309(2)	O3−Cu2−O63	117.34(8)
Cu2−O63	1.966(2)	O3−Cu2−O64	171.78(8)
Cu2−O64	2.555(2)	O3−Cu2−N5	92.81(9)
Cu2−N4	2.015(3)	O3−Cu2−N4	92.29(9)
Cu2−N5	2.015(3)	O3−Cu2−N6	90.47(9)
Cu2−N6	2.030(3)	O63−Cu2−N5	96.37(10)
O1−C1	1.362(4)	O63−Cu2−N4	150.30(10)
O3−C7	1.361(4)	O63−Cu2−N6	93.77(10)
O61−C61	1.273(4)	O63−Cu2−O64	56.71(9)
O62−C61	1.254(4)	O64−Cu2−N5	93.55(10)
O63−C63	1.273(4)	O64−Cu2−N4	93.61(9)
O64−C63	1.251(4)	O64−Cu2−N6	84.54(9)
		N4−Cu2−N5	83.30(11)
O1−Cu1−N1	93.93(10)	N4−Cu2−N6	83.44(11)
O1−Cu1−N2	90.18(10)	N5−Cu2−N6	166.46(11)
O1−Cu1−N3	90.49(9)	O61−C61−O62	121.8(3)
O1−Cu1−O61	110.82(9)	O62−C61−C62	120.6(3)
O1−Cu1−O62	166.96(9)	O61−C61−C62	117.6(3)
O61−Cu1−O62	56.16(9)	O63−C63−O64	122.1(3)
O61−Cu1−N1	155.20(11)	O64−C63−C64	121.1(3)
O61−Cu1−N2	95.45(11)	O63−C63−C64	116.8(3)
O61−Cu1−N3	98.55(10)		

naphthalenediol (Cu−O = 2.28 and 2.31 Å) are coordinated in the Jahn−Teller axes of the Cu^{II} ions. The two Cu^{II} ions are not in the naphthalene plane but oriented to opposite sides relative to the naphthalene plane (Figure 3b) demonstrating some degree of flexibility of the Cu^{II} polyhedra especially at the benzylic carbon atoms. The 1,8-naphthalenediol backbone affords an intramolecular Cu−Cu distance of 6.32 Å. The labile acetates are at the potential binding sites for the DNA phosphate oxygen donor atoms. The O···O distances between the two acetates are 7.02, 8.88, 8.91, and 10.85 Å. These distances in conjunction with the flexibility at the benzylic carbon atoms hint at the capability of **Cu$_2$**$^{2+}$ to coordinate to two neighboring phosphates of the DNA backbone by molecular recognition.

The magnetic measurements reveal an almost temperature-independent effective magnetic moment, μ_{eff}, of 2.65 μ_B (Figure 4). Simulations using the adequate spin Hamiltonian ($H = -2J\mathbf{S}_1\mathbf{S}_2$) for dinuclear Cu^{II}_2 complexes provide a good reproduction of the experimental data with an almost vanishing coupling constant $J = -0.1$ cm^{-1}. This small coupling behavior is consistent with the Cu−O^{ar} bonds being in the Jahn−Teller axes. Thus, despite the long Cu−O^{ar} bonds, the magnetic d($x^2 - y^2$) orbitals are of δ symmetry with respect to the Cu−O^{ar} bonds and thus nonbonding.

As a prerequisite for studying the interaction with DNA under physiological conditions, **Cu$_2$**($OAc)_2$ is highly soluble in water and buffer solutions. We attribute this to a loss of bound acetate resulting in a hydrated form of **Cu$_2$**$^{2+}$. As crystallization of **Cu$_2$**$^{2+}$-bound DNA seems to be elusive due to the sequence-unspecific binding of **Cu$_2$**$^{2+}$ to DNA providing only statistical mixtures of **Cu$_2$**$^{2+}$-bound DNA, we evaluated the binding of

DOI: 10.1021/ic5028465
Inorg. Chem. 2015, 54, 2679−2690

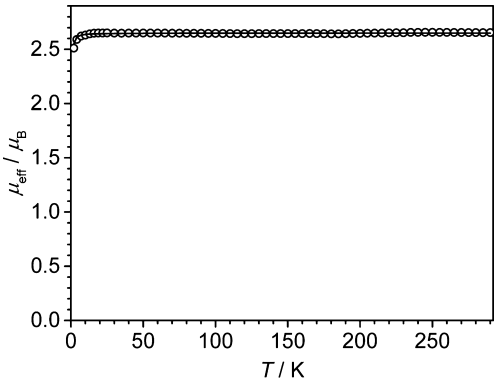

Figure 4. Temperature dependence of μ_{eff} for $Cu_2(OAc)_2$. Solid line corresponds to the best fit to the spin Hamiltonian using $J = -0.1$ cm^{-1}, $g = 2.163$.

Cu_2^{2+} to DNA by independent biochemical, spectroscopic, and single-molecule methods.

Interaction with DNA Studied by Gel Electrophoresis. Although the dinuclear copper complex was chosen as the first complex of this family of complexes to strongly bind to DNA and not to exhibit a strong hydrolytic cleavage ability, we first tested the ability of $Cu_2(OAc)_2$ for hydrolytic cleavage. In this respect, plasmid DNA (100 μM DNA phosphates) was incubated with $Cu_2(OAc)_2$ and studied by agarose gel electrophoresis. Addition of copper chloride or MOM_2tom^{Me} was studied as reference (Figure 5). Circular plasmid DNA can adopt different topoisomers. The supercoiled plasmid is a tense topoisomer that results from partial unwinding and is the predominant form in bacteria. It migrates fastest on an agarose gel due to its compactness. The supercoiled topoisomer of our 3 kb (kilo base pairs) plasmid had a similar mobility as the 2 kb linear marker fragment. If one phosphodiester bond is hydrolyzed, a nick is introduced and the supercoiled plasmid relaxes into the open-circular form, which migrates slower on agarose gels similar to the 4 kb linear marker fragment. If both DNA strands are hydrolyzed in close proximity the circular plasmid is converted into the linear form as observed after digestion with the restriction enzyme *Eco*RI (Figure 5, Eco).

While 5% open-circular plasmid DNA were already present without addition (0 μM), 10−50 μM $Cu_2(OAc)_2$ increased the share of open-circular plasmid DNA slightly but significantly to 12−14% (Figure 5, quantification in Figure S2a, Supporting Information). Addition of comparable concentrations of copper chloride or MOM_2tom^{Me} did not alter the amount of open-circular plasmid DNA. The linear form was not observed after addition of $Cu_2(OAc)_2$, indicating that Cu_2^{2+} did not cause massive hydrolysis. This indicates that Cu_2^{2+} hydrolyzes DNA with very low frequency. Although this is only a weak acceleration of hydrolytic phosphodiester cleavage, it is a clear indication that Cu_2^{2+} binds to the phosphate backbone of DNA.

Most interestingly, an unknown behavior has been observed for concentrations above 100 μM $Cu_2(OAc)_2$. As can be seen in Figure 5, the dark spots from the ethidium fluorescence, which indicate the location of the DNA, persisted in the loading pocket for concentrations of 100 and 200 μM. This indicates that the DNA was not entering the gel. Moreover, at 500 μM no ethidium fluorescence was observed, although a DNA−Cu_2^{2+} precipitate could be observed in the loading pocket

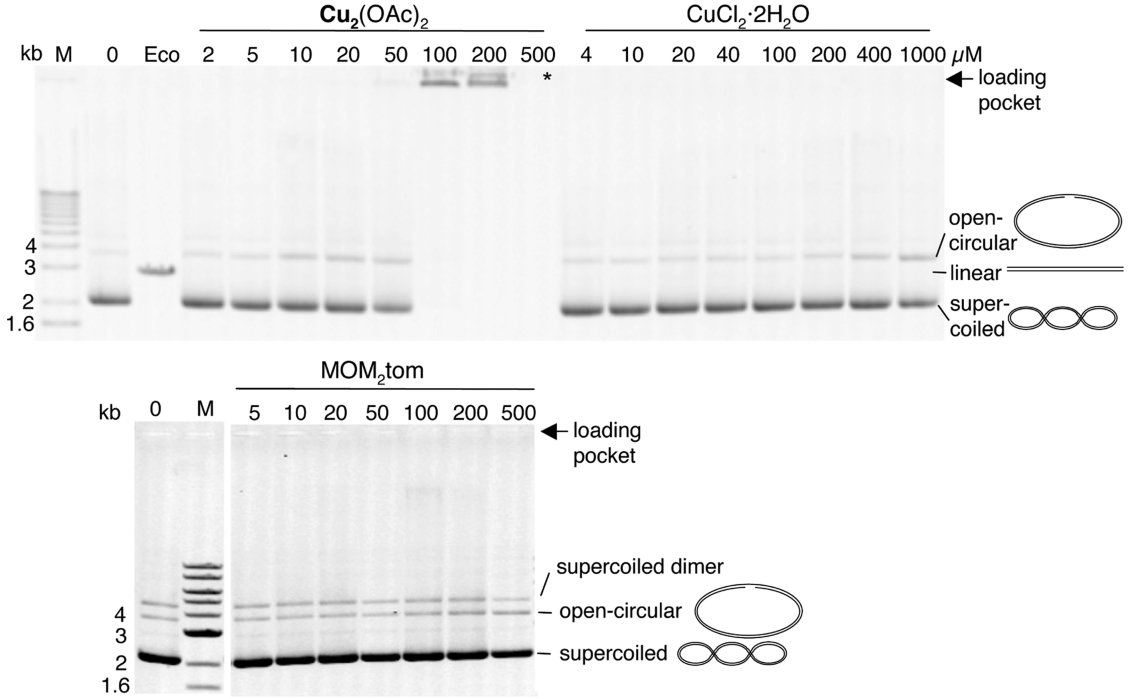

Figure 5. Interaction of $Cu_2(OAc)_2$ with plasmid DNA. Plasmid DNA incubated with the indicated concentrations of $Cu_2(OAc)_2$, copper chloride ($CuCl_2·2H_2O$), or MOM_2tom^{Me} for 1 h at 37 °C was separated by agarose gel electrophoresis after transfer into the loading pockets (arrows) and DNA stained with ethidium. DNA hydrolysis in the supercoiled topoisomer leads to the slight increase in the amount of open-circular DNA observed at 10−50 μM $Cu_2(OAc)_2$. The mobility of the DNA is lost above at 100 μM $Cu_2(OAc)_2$, because it does not leave the loading pocket. (*) Plasmid DNA is present but could not be detected with ethidium. (0) no additions; (Eco) plasmid DNA linearized by the restriction enzyme *Eco*RI; (M) marker; kb kilo base pairs.

DOI: 10.1021/ic5028465
Inorg. Chem. 2015, 54, 2679−2690

(Figure 5 asterisk). By contrast, neither copper chloride nor MOM_2tom^{Me} did prevent the migration of the DNA.

The aromatic dye bromphenol blue was present in the loading buffer to monitor the progress of the electrophoresis in an additional experiment. Only in the presence of 100−500 μM $\mathbf{Cu_2}(OAc)_2$ bromphenol blue stayed in the loading pocket (Figure S2b, Supporting Information). This indicates that an immobile aggregate of DNA, $\mathbf{Cu_2}^{2+}$, and bromphenol blue has formed. Even in the absence of bromphenol blue precipitates were visible in the loading pockets of the gel at 500 μM $\mathbf{Cu_2}(OAc)_2$ or above in the presence of 100 μM DNA bases/phosphates. These data indicate that DNA is aggregated by $\mathbf{Cu_2}^{2+}$ at high concentrations and not able to enter the agarose gel.

The observation that DNA is not entering the gel may be explained either by an increased size of the DNA so that it is too large to pass through the gel or by a charge neutrality so that the electric field in the gel electrophoresis experiment does not attract the DNA to enter the gel. The latter would indicate that all negatively charged phosphates of the DNA are complexed by a Cu^{II} ion of $\mathbf{Cu_2}^{2+}$. However, this should be a gradual effect with increasing concentration of $\mathbf{Cu_2}^{2+}$, but no indication of a reduced velocity of DNA migration can be detected at lower concentrations. This implies that the presence of $\mathbf{Cu_2}^{2+}$ at high concentration induces the formation of a firm DNA network, so that the resulting conglomerate is too large to pass through the gel.

DNA Binding Studies in Solution by UV−Vis and NMR Spectroscopies. As the gel electrophoresis experiments showed not only that $\mathbf{Cu_2}(OAc)_2$ possesses only a moderate hydrolytic activity but also that there is also a significant binding of $\mathbf{Cu_2}^{2+}$ that unexpectedly causes interconnection of DNA plasmids, we wanted to quantify this DNA binding. In this respect, we incubated the plasmid DNA (600 μM DNA phosphates) with various amounts of $\mathbf{Cu_2}(OAc)_2$ (100−3000 μM). The $\mathbf{Cu_2}^{2+}$-bound DNA was precipitated by 70% ethanol and 75 mM $NaClO_4$. NaOAc in the standard DNA precipitation protocol was replaced by $NaClO_4$ because ClO_4^- does not complex Cu^{II} in contrast to OAc^-. Pellets were washed and redissolved in either buffer or water, and the absorption at 356 nm (28 100 cm^{-1}) was measured by UV−vis spectroscopy. $\mathbf{Cu_2}(OAc)_2$ shows a strong absorbance at this wavelength (Figure 2 inset), while absorption of DNA is negligible. However, the redissolved pellets exhibited a significant background absorption at high wavelengths, where no DNA absorption is feasible. This background absorption is more intense than the Cu^{II} d−d bands and does not possess their characteristic signature. Moreover, this background absorption increased with increased $\mathbf{Cu_2}(OAc)_2$ concentrations. We assign this background to scattering effects from nanosized objects. The only nanosized objects present are the DNA molecules, but they are not large enough for the scattering observed. The increased scattering by increased $\mathbf{Cu_2}(OAc)_2$ concentration corroborates the results observed by gel electrophoresis that $\mathbf{Cu_2}^{2+}$-bound DNA molecules interconnect.

In another attempt to quantify this DNA binding, we performed titration experiments of $\mathbf{Cu_2}(OAc)_2$ with DNA.[38] DNA binding by intercalation is indicated in these experiments by an intensity decrease of the intercalating chromophore. In our experiments using low DNA concentrations, a significant intensity increase of the absorption of $\mathbf{Cu_2}^{2+}$ at 28 100 cm^{-1} (356 nm) was observed providing strong evidence for a nonintercalating binding mode. However, at moderate to high DNA concentrations, a strong scattering background prevented a quantitative analysis of the DNA binding. Efforts to separate the scattering background led to different results for various titration experiments. Thus, the strong interconnecting tendency of $\mathbf{Cu_2}^{2+}$-bound DNA prevented further analysis of this binding.

The same holds true for NMR experiments. ^{31}P NMR has been proven as a valuable tool to examine the binding of paramagnetic metal ions to the phosphates of DNA.[39] However, even at such low DNA concentrations that needed 3 days acquisition time on a 600 MHz NMR spectrometer for the $\mathbf{Cu_2}^{2+}$-free reference measurements a precipitate resulted by adding $\mathbf{Cu_2}^{2+}$ (1:10 ratio). Thus, NMR measurements in solution for further evaluation of this binding are also prevented.

DNA binding by AFM Imaging. Although conventional methods for studying DNA binding provide strong evidence for a strong binding of $\mathbf{Cu_2}^{2+}$, these methods do not allow a more detailed study as $\mathbf{Cu_2}^{2+}$-bound DNA seems to induce intermolecular DNA entanglements. Thus, we applied single-molecule methods, namely, atomic force microscopy (AFM), optical tweezers (OT), and magnetic tweezers (MT) DNA stretching experiments, to investigate this binding in more detail. First, we investigated the DNA binding properties of $\mathbf{Cu_2}(OAc)_2$ by AFM imaging.[40] Linear λ-DNA was incubated with 50 and 200 μM $\mathbf{Cu_2}(OAc)_2$ and imaged by AFM in tapping mode of operation under ambient conditions. In Figure 6, representative AFM images of the untreated reference λ-DNA (Figure 6a) as well as $\mathbf{Cu_2}(OAc)_2$-treated λ-DNA samples (Figure 6b and 6c) are shown.

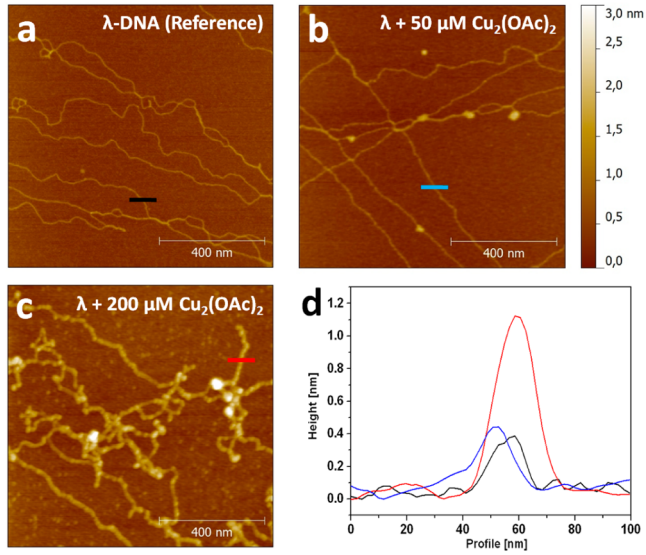

Figure 6. DNA binding of $\mathbf{Cu_2}(OAc)_2$ studied by AFM. (a−c) AFM topography images (1 μm × 1 μm) with a z scale of 3.0 nm. (a) Untreated linear λ-DNA (Reference). (b) $\mathbf{Cu_2}(OAc)_2$-treated λ-DNA (50 μM) with local intra- and interstrand entanglements. (c) $\mathbf{Cu_2}(OAc)_2$-treated λ-DNA (200 μM) exhibiting fully complexed DNA with local intra- and interstrand coiling induced by interaction with the metal complex. It should be noted that the bright spots do not represent the copper complexes alone but copper complex-induced DNA coils and knots. (d) AFM topography cross sections as indicated in a−c displaying an effective corrugation height of 0.4−0.5 and 1.2 nm for untreated λ-DNA and the $\mathbf{Cu_2}^{2+}$-bound DNA, respectively. Local entanglements can be as large as 3.0−4.0 nm.

DOI: 10.1021/ic5028465
Inorg. Chem. 2015, 54, 2679−2690

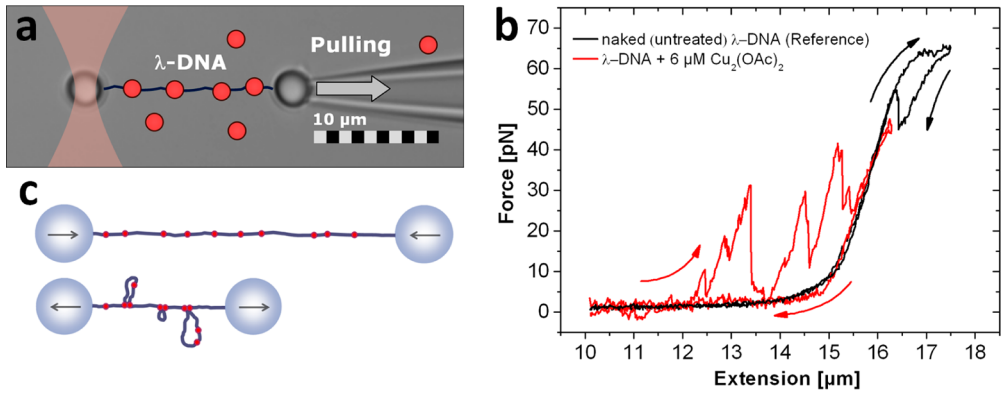

Figure 7. DNA stretching experiments with optical tweezers (OT). (a) OT micrograph setup: One single λ-DNA is immobilized between two microbeads (one is fixed by a micropipette and the other inside the optical trap). (b) Force–extension curves with untreated λ-DNA (black curve) and $Cu_2(OAc)_2$-treated λ-DNA (red curve). In contrast to the reference curve where a significant increase of the force can be discerned at an extension approaching the molecular contour length, a multipeak signature can be detected for $Cu_2(OAc)_2$-treated λ-DNA. (c) Molecular model that attributes these peaks to $Cu_2(OAc)_2$-induced DNA–intrastrand interactions and local DNA entanglements that shorten the global molecular contour length and resist a maximum force before they break.

Whereas native λ-DNA exhibits a linear and smooth appearance, distinct corrugations and aggregation spots can be discerned in Figure 6b and 6c, indicating Cu_2^{2+} binding with local DNA entanglements or partial folding of dsDNA. In Figure 6c the complete DNA strand is affected by the Cu_2^{2+} binding, which could also be quantified by the measured effective height of the complexed DNA strand as shown in Figure 6d. Whereas native λ-DNA usually displays an effective corrugation height of 0.4–0.5 nm, the DNA height at high Cu_2^{2+} concentration increases to 1.2 nm with distinct aggregative spots, yielding a height of up to 3.0–4.0 nm. Since this observation could be made using either Tris buffer or ultrapure water as the solvent and the samples were rigorously washed after the incubation steps (what can also be inferred from Figure 6a) we can exclude salt aggregation effects of the buffer. These single-molecule measurements corroborate the observations from the gel electrophoresis and the solution spectroscopic experiments that the complex Cu_2^{2+} strongly interacts with DNA. Furthermore, our AFM experiments support Cu_2^{2+}-induced DNA intra- and interstrand interactions and bridging as it was concluded from the gel electrophoresis and the solution spectroscopic experiments.

DNA Binding by Optical Tweezers Nanomechanics. In addition to AFM, we investigated the interaction of $Cu_2(OAc)_2$ with dsDNA by molecular stretching experiments with optical tweezers (OT). Here, one single λ-DNA molecule was functionalized on both ends with multibiotins, immobilized between two streptavidin-coated polystyrene microbeads, and subsequently mechanically (over)stretched in force spectroscopy experiments by OT (Figure 7a).[25,41] These nanomechanical experiments allow insights into the structure and force mechanics of long biopolymers and their interplay with binding agents.[25] Reference force/extension experiments exhibit a smooth, nonlinear force increase when stretching the untreated λ-DNA (Figure 7b). A measurable force starts to significantly increase at an extension approaching the molecular contour length of 16.4 μm (Figure 7b, black curve). The plateau that is reached at 64 pN is due to the onset of local melting processes that occur during overstretching.[42] After relaxing the DNA molecule again, the force–extension curve compares almost with the one from the extensional process with the exception of a small hysteretic regime reflecting nonequilibrium processes during the first stages of rehybridization.

Upon adding a solution of 6 μM $Cu_2(OAc)_2$ and waiting typically a few (>2) minutes, the very same DNA molecule was stretched and relaxed again (Figure 7b, red curve). Now, several peaks can readily be discerned in the stretching curve. Each of these peaks can be attributed to Cu_2^{2+}-induced DNA–intrastrand interactions and local DNA entanglements that shorten the global molecular contour length and resist a maximum force before they break (Figure 7c), conceptually very similar to protein unfolding experiments with AFM.[43] These force peak values are typically between 10 and 40 pN, which are in the range of 3–6 times the force of a hydrogen bond.[44] This may lead to the conclusion that Cu_2^{2+}-bound DNA molecules are attracting and binding each other by π–π stacking interactions of the aromatic rings of their naphthalene backbone and/or their pyridyl rings of the pendant arms. Importantly, the corresponding relaxation curves always remained perfectly superimposed with the reference relaxation curve. This observation fully complies with the AFM observation, where the binding of Cu_2^{2+} to dsDNA also induces distinct local entanglements of the DNA. Interestingly, during immediate, subsequent, and ongoing stretching experiments the same overall "multipeak" signature can be detected again, however, appearing at different extension lengths. This of course can be explained by a permutation of the DNA–intrastrand interaction mediated by statistically distributed Cu_2^{2+} binding along the DNA strand. It is worth noting that removing the Cu_2^{2+} solution and additional rinsing with buffer or ultrapure water did not alter the multipeak signature at all, pointing to a firm and irreversible binding of Cu_2^{2+} to DNA.

In order to relate the observed phenomenon unequivocally to the binding of Cu_2^{2+} to DNA, control experiments with copper(II) acetate instead of $Cu_2(OAc)_2$ in comparable concentrations have been conducted. They did not show any force peaks during DNA stretching and no deviation from the original force–extension curve of the untreated λ-DNA (data not shown).

DNA Binding by Magnetic Tweezers. In addition to our AFM and OT experiments we conducted magnetic tweezers (MT) experiments on single torsionally constrained short DNA fragments. Such experiments allow nanomechanical force

DOI: 10.1021/ic5028465
Inorg. Chem. 2015, 54, 2679–2690

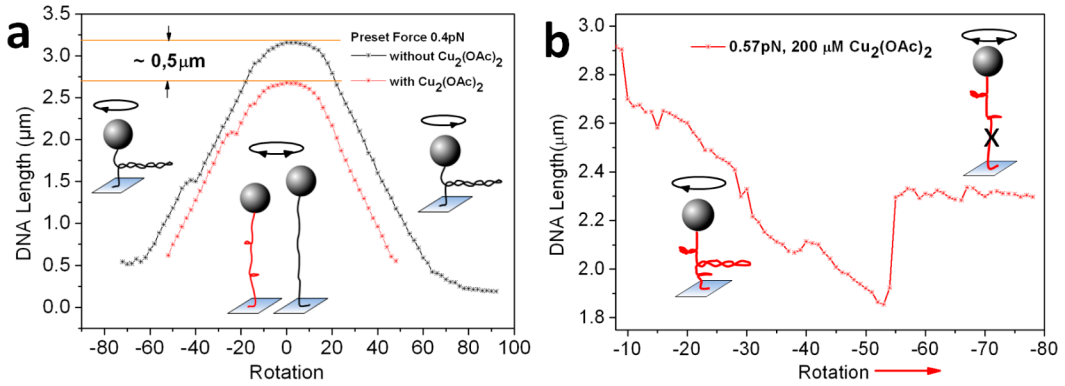

Figure 8. DNA stretching experiments with magnetic tweezers (MT). (a) MT "hat" curve showing the effective length reduction of a torsionally constrained, 3.25 μm long DNA with plectonemic superspiralization due to DNA overwinding (black curve). Upon adding 200 μM $\mathbf{Cu_2}(OAc)_2$ a similar hat curve with a ~0.5 μm smaller effective length could be measured (red curve). (b) In rare cases hydrolytic phosphodiester cleavage of the DNA backbone and introduction of a DNA nick could be observed. During DNA overwinding, suddenly the effective DNA length increased to a certain value that could not any more be affected by further rotation.

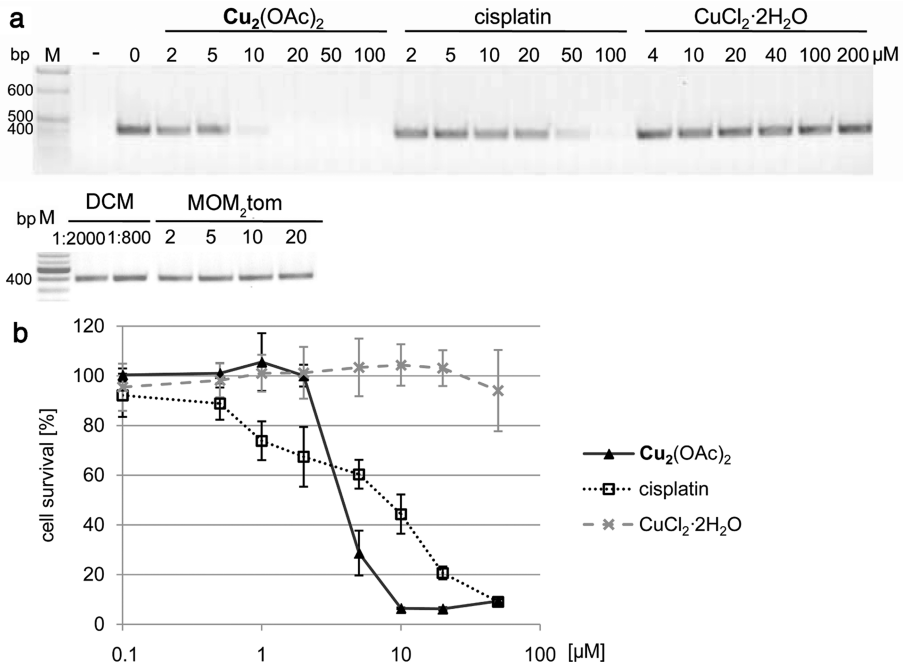

Figure 9. Inhibition of DNA synthesis by $\mathbf{Cu_2}(OAc)_2$ and cytotoxicity of $\mathbf{Cu_2}(OAc)_2$ in human cancer cells. (a) PCR reactions with the indicated additions were analyzed by agarose gel electrophoresis. Ten micromolar $\mathbf{Cu_2}(OAc)_2$ inhibited the DNA polymerase, while copper chloride ($CuCl_2 \cdot 2H_2O$) or MOM_2tom^{Me} were without effect: (−) no DNA; (M) marker; (bp) base pairs; (DCM) dichloromethane was added in the indicated concentration because it was used as a solvent for MOM_2tom^{Me}. (b) Survival of HeLa cells incubated with the indicated additions was analyzed photometrically after 3 days by staining of proteins with sulforhodamine B. Values without additions were set to 100% and used for normalization. Ten micromolar $\mathbf{Cu_2}(OAc)_2$ killed HeLa cells. Shown are means ± SD, n = 3.

spectroscopy experiments with single DNA strands introducing torsional molecular overwinding and manipulative superspiralization.[45] After having immobilized a DNA fragment via their ends between a surface and a superparamagnetic bead (Figure 8a, inset) an external magnetic field is applied, which extends the DNA in the axial direction.

In addition to this axial magnetic force the magnetic field exerts also a radial force component that interacts with the magnetic dipole of the superparamagnetic bead and allows a controlled rotational motion of the bead in both directions. In case of a (i) torsionally constrained DNA immobilization and (ii) nick-free double-stranded DNA structure, the DNA gets overwound and undergoes plectonemic superspiralization accompanied by a reduction of the effective length (= distance surface−bead). This can be seen in Figure 8a (black curve), where such a characteristic "hat" curve is shown.[45] In this experiment the preset stretching force was set to 0.4 pN, leading to an effective contour length of 3.25 μm. Upon adding 200 μM $\mathbf{Cu_2}(OAc)_2$ the same experiment was conducted again, which resulted in a similar "hat" curve that was, however, shifted by ~0.5 μm to smaller effective lengths. This length reduction can be explained as a successful binding of $\mathbf{Cu_2}^{2+}$ to DNA accompanied by DNA−intrastrand interaction as it has also been detected in our OT experiments. In contrast to OT, where those intrastrand interactions (10−40 pN) could be broken up by an external OT force, the limited maximum force in MT (~20 pN) prevented a complete disentanglement of the DNA, therefore resulting in an overall effective length

DOI: 10.1021/ic5028465
Inorg. Chem. 2015, 54, 2679−2690

reduction. In rare cases, long-term MT experiments on the very same $Cu_2(OAc)_2$-treated DNA molecule yielded evidence of rare hydrolytic phosphodiester cleavage of the DNA backbone (Figure 8b) as discussed above in our gel electrophoresis experiments. There, during DNA overwinding, suddenly the effective DNA length increased to a certain value that could not any more be affected by further rotation (clock or counterclockwise). This phenomenon can be explained by the introduction of a nick in a DNA strand as a result of a hydrolytic phosphodiester cleavage conceptually similar to the functional activity of topoisomerases as it could be also detected by MT.[46] The result is an abolished torsional constriction of the DNA leaving the biopolymer in an idle state where no torsional forces can be applied to (Figure 8b, inset).

Inhibition of DNA synthesis. The binding of Cu_2^{2+} to DNA should prevent the interaction of DNA with DNA polymerases due to sterical hindrances and therefore should prevent DNA synthesis. A very efficient way to use DNA polymerases for the synthesis of DNA in test tubes is the polymerase chain reaction (PCR). A template DNA is amplified using two oligonucleotide primers, which hybridize with the DNA as the starting point for the Taq DNA polymerase. DNA is amplified in repeated cycles of denaturation of double-stranded DNA, primer binding, and DNA synthesis. In order to evaluate the effect of Cu_2^{2+}-bound DNA on DNA synthesis, polymerase chain reactions were performed in the presence of $Cu_2(OAc)_2$, copper chloride, MOM_2tom^{Me}, or cisplatin (Figure 9a). A DNA fragment of about 400 bp was amplified in the absence of additions (Figure 9a, 0). Interestingly, the PCR reaction was strongly affected at 10 μM $Cu_2(OAc)_2$, and DNA was not amplified at 20 μM or above. Neither copper chloride nor MOM_2tom^{Me} affected DNA synthesis at these concentrations, excluding nonspecific effects of Cu^{II} or MOM_2tom^{Me} on the DNA polymerase. Comparably, 50 μM cisplatin was required for strong inhibition of the DNA polymerase. These experiments prove that Cu_2^{2+} inhibits DNA synthesis at lower concentrations than cisplatin. This inhibition can be caused by the binding of Cu_2^{2+} to DNA, but these experiments do not allow us to exclude that inhibition is caused by an interaction of Cu_2^{2+} with the DNA polymerase.

Cytotoxicity to Human Cancer Cells. As the PCR experiments show that Cu_2^{2+} is a potent inhibitor of DNA synthesis under those conditions, we tested its cytotoxicity. Equal numbers of HeLa human cancer cells were seeded into 96-well plates and allowed to grow for 24 h. Afterward, they were incubated for 3 days without additions or with 0.1−50 μM $Cu_2(OAc)_2$, copper chloride, or cisplatin. Cell survival was assayed microscopically (Figure S3, Supporting Information). Healthy cells are attached to the surface and spread out. Healthy HeLa cells covered a large fraction of the well in cells incubated with copper chloride or 0.5 or 2 μM $Cu_2(OAc)_2$. By contrast, hardly any healthy cells were seen after incubation with 10 or 20 μM $Cu_2(OAc)_2$, but round stressed or dead cells were visible. As a quantitative measure for cell numbers their proteins were stained with sulforhodamine B and the absorption measured photometrically in an ELISA plate reader (Figure 9b). HeLa cells survived 2 μM $Cu_2(OAc)_2$ but were killed by 10 μM. Cisplatin had a more gradual effect on HeLa cells with cytotoxic effects starting at 1 μM and maximal effects at 20 μM. Similar results were obtained by testing cell survival with the XTT assay (data not shown), which measures metabolic reduction of a tetrazolium reagent to a formazan. As concentrations of 10 μM Cu_2^{2+} inhibited DNA synthesis and resulted in complete cell death, our data suggest that (i) Cu_2^{2+} is membrane permeable, which is a prerequisite for developing novel anticancer drugs, and (ii) binding of Cu_2^{2+} to DNA inhibits DNA polymerase and is the reason for cell death in HeLa cells.

CONCLUSIONS

In summary, we developed by rational design a new dinuclear complex family with the objective of binding to two neighboring phosphates in the backbone of dsDNA yielding a cytotoxic effect to human cancer cells in analogy to the nucleobase-binding family of cisplatin anticancer drugs. Several independent experiments at the single-molecule level and ensemble experiments in solution provide strong evidence for a severe, irreversible binding of the dinuclear $Cu_2(OAc)_2$ complex to DNA. It should be noted that crystallization of a Cu_2^{2+}-bound DNA is elusive as Cu_2^{2+} does not bind to DNA in a sequence-specific manner. Thus, only statistical mixtures of Cu_2^{2+}-bound DNA molecules are present in solution that cannot crystallize. Therefore, only the application of a combination of biochemical, spectroscopic, and single-molecule methods allows obtaining insight into the binding of Cu_2^{2+} to DNA.

The strong inhibition of DNA synthesis and the strong cytotoxicity effects of $Cu_2(OAc)_2$ compared to cisplatin presupposes an efficient Cu_2^{2+}-DNA interaction in vitro and in living cells. The weak but measurable ability of Cu_2^{2+} to cleave DNA demonstrates its binding capability to the DNA phosphates, where the phosphate oxygen atoms on the DNA surface are pointing outward. Cu_2^{2+} binding to these phosphate oxygen atoms results in a decoration of the DNA surface with naphthalene rings making the hydrophilic DNA backbone more hydrophobic. In these aqueous solutions $\pi-\pi$ or other van-der-Waals-like interactions of the naphthalene rings of phosphate-bound Cu_2^{2+} enable intramolecular DNA entanglements as evidenced by the knot and coil formations by AFM and OT stretching experiments. Intermolecular DNA entanglements could be evidenced in gel electrophoresis experiments and by the strong scattering effects in UV−vis spectroscopy experiments. Currently, we are investigating the influence, binding, and cytotoxicity of various other metal ions in $[(tom^{Me})M_2]^{n+}$ for binding to DNA and their potential for oncogenic applications.

ASSOCIATED CONTENT

Supporting Information

Thermal ellipsoid plot, quantification of gel electrophoresis, microscopy pictures of HeLa cell death studies, NMR spectra. This material is available free of charge via the Internet at http://pubs.acs.org.

AUTHOR INFORMATION

Corresponding Author

*E-mail: thorsten.glaser@uni-bielefeld.de.

Notes

The authors declare no competing financial interest.

ACKNOWLEDGMENTS

Financial support by the Deutsche Forschungsgemeinschaft within the Collaborative Research Center SFB613 (project A9) and Bielefeld University is gratefully acknowledged.

DOI: 10.1021/ic5028465
Inorg. Chem. 2015, 54, 2679−2690

REFERENCES

(1) (a) Lippert, B. *Coord. Chem. Rev.* **2000**, *200*−*202*, 487−516. (b) Derose, V. J.; Burns, S.; Kim, N.-K.; Vogt, N. In *Comprehensive Coordination Chemistry II*; McCleverty, J. A., Meyer, T. J., Eds.; Elsevier, Ltd.: Oxford, 2004; Vol. *8*, pp 787−813. (c) In *Nucleic Acid-Metal Ion Interactions*; Hud, N. V., Ed.; Royal Society of Chemistry: Cambridge, 2008. (d) In *Interplay between metal ions and nucleic acids*; Sigel, A., Sigel, H., Sigel, R. K. O., Eds.; Springer: Dordrecht, New York, 2012.

(2) (a) Scott, W. G.; Murray, J. B.; Arnold, J. R. P.; Stoddard, B. L.; Klug, A. *Science.* **1996**, *274*, 2065−2069. (b) Rulisek, L.; Sponer, J. *J. Phys. Chem. B* **2003**, *107*, 1913−1923. (c) Alexandre, S. S.; Murta, B. J.; Soler, J. M.; Zamora, F. *Phys. Rev. B* **2011**, *84*, 045413. (d) Sigel, H.; Amsler, P. E. *J. Am. Chem. Soc.* **1976**, *98*, 7390−7400. (e) Cartwright, B. A.; Goodgame, D.; Jeeves, I.; Skapski, A. C. *Biochim. Biophys. Acta* **1977**, *477*, 195−198. (f) Fischer, B. E.; Bau, R. *Inorg. Chem.* **1978**, *17*, 27−34.

(3) Erkkila, K. E.; Odom, D. T.; Barton, J. K. *Chem. Rev.* **1999**, *99*, 2777−2795.

(4) Claussen, C. A.; Long, E. C. *Chem. Rev.* **1999**, *99*, 2797−2816.

(5) (a) Fichtinger-Schepman, A. M. J.; Vanderveer, J. L.; Denhartog, J. H. J.; Lohman, P. H. M.; Reedijk, J. *Biochemistry.* **1985**, *24*, 707−713. (b) Sherman, S. E.; Gibson, D.; Wang, A. H. J.; Lippard, S. J. *Science* **1985**, *230*, 412−417.

(6) Yang, D.; von Boom, S. S. G. E.; Reedijk, J.; Van Boom, J. H.; Wang, A. H.-J. *Biochemistry.* **1995**, *34*, 12912−12920.

(7) (a) Takahara, P. M.; Rosenzweig, A. C.; Frederick, C. A.; Lippard, S. J. *Nature* **1995**, *377*, 649−652. (b) Takahara, P. M.; Frederick, C. A.; Lippard, S. J. *J. Am. Chem. Soc.* **1996**, *118*, 12309−12321. (c) Gelasco, A.; Lippard, S. J. *Biochemistry.* **1998**, *37*, 9230−9239.

(8) Jamieson, E. R.; Lippard, S. J. *Chem. Rev.* **1999**, *99*, 2467−2498.

(9) (a) Pinto, A. L.; Lippard, S. J. *Proc. Natl. Acad. Sci. U.S.A.* **1985**, *82*, 4616−4619. (b) Suo, Z.; Lippard, S. J.; Johnson, K. A. *Biochemistry.* **1999**, *38*, 715−726. (c) Wang, D.; Lippard, S. J. *Nat. Rev. Drug Discovery* **2005**, *4*, 307−320. (d) Jung, Y.; Lippard, S. J. *Chem. Rev.* **2007**, *107*, 1387−1407. (e) Tornaletti, S.; Patrick, S. M.; Turchi, J. J.; Hanawalt, P. C. *J. Biol. Chem.* **2003**, *278*, 35791−35797. (f) Jung, Y. W.; Lippard, S. J. *J. Biol. Chem.* **2003**, *278*, 52084−52092.

(10) (a) Galanski, M. *Recent Pat. Anti-Cancer Drug Discovery* **2006**, *1*, 285−295. (b) In *Cisplatin-Chemistry and Biochemistry of a Leading Anticancer Drug*; Lippert, B., Ed.; Wiley VCH: New York, 1999. (c) Timerbaev, A. R.; Hartinger, C. G.; Aleksenko, S. S.; Keppler, B. K. *Chem. Rev.* **2006**, *106*, 2224−2248.

(11) Galluzzi, L.; Senovilla, L.; Vitale, I.; Michels, J.; Martins, I.; Kepp, O.; Castedo, M.; Kroemer, G. *Oncogene* **2012**, *31*, 1869−1883.

(12) (a) Pabla, N.; Dong, Z. *Kidney Int.* **2008**, *73*, 994−1007. (b) Miller, R. P.; Tadagavadi, R. K.; Ramesh, G.; Reeves, W. B. *Toxins* **2010**, *2*, 2490−2518.

(13) Ho, Y. P.; Au-Yeung, S. C. F.; To, K. K. W. *Med. Res. Rev.* **2003**, *23*, 633−655.

(14) (a) Lerman, L. S. *J. Mol. Biol.* **1961**, *3*, 18−30. (b) Kelland, L. *Nat. Rev. Cancer.* **2007**, *7*, 573−584.

(15) (a) Wilcox, D. E. *Chem. Rev.* **1996**, *96*, 2435−2458. (b) Cowan, J. A. *Chem. Rev.* **1998**, *98*, 1067−1087.

(16) Weston, J. *Chem. Rev.* **2005**, *105*, 2151−2174.

(17) (a) Gajewski, E.; Aruoma, O. I.; Dizdaroglu, M.; Halliwell, B. *Biochemistry* **1991**, *30*, 2444−2448. (b) Parkin, G. *Chem. Rev.* **2004**, *104*, 699−767. (c) Aoki, S.; Kimura, E. *Chem. Rev.* **2004**, *104*, 769−787. (d) Liu, C.; Wang, M.; Zhang, T.; Sun, H. *Coord. Chem. Rev.* **2004**, *248*, 147−168. (e) Liu, C.; Wang, L. *Dalton Trans.* **2009**, 227−239.

(18) Williams, N. H.; Takasaki, B.; Wall, M.; Chin, J. *Acc. Chem. Res.* **1999**, *32*, 485−493.

(19) Mitic, N.; Smith, S. J.; Neves, A.; Guddat, L. W.; Gahan, L. R.; Schenk, G. *Chem. Rev.* **2006**, *106*, 3338−3363.

(20) (a) Desbouis, D.; Troitsky, I. P.; Belousoff, M. J.; Spiccia, L.; Graham, B. *Coord. Chem. Rev.* **2012**, *256*, 897−937. (b) Mancin, F.; Scrimin, P.; Tecilla, P. *Chem. Commun.* **2012**, *48*, 5545−5559. (c) Zhao, M.; Wang, H.-B.; Ji, L.-N.; Mao, Z.-W. *Chem. Soc. Rev.* **2013**, *42*, 8360−8375. (d) de Souza, B.; Heying, R.; Bortoluzzi, A. J.; Domingos, J. B.; Neves, A. *J. Mol. Catal. A: Chem.* **2015**, *397*, 76−84.

(21) Tjioe, L.; Meininger, A.; Joshi, T.; Spiccia, L.; Graham, B. *Inorg. Chem.* **2011**, *50*, 4327−4339.

(22) Glaser, T.; Liratzis, I. *Synlett* **2004**, *4*, 735−737.

(23) Komatsu, K.; Kikuchi, K.; Kojima, H.; Urano, Y.; Nagano, T. *J. Am. Chem. Soc.* **2005**, *127*, 10197−10204.

(24) The program package JulX was used for spin-Hamiltonian simulations and fittings of the data by a full-matrix diagonalization approach. Bill, E. Unpublished results.

(25) Sischka, A.; Toensing, K.; Eckel, R.; Wilking, S. D.; Sewald, N.; Ros, R.; Anselmetti, D. *Biophys. J.* **2005**, *88*, 404−411.

(26) Sischka, A.; Kleimann, C.; Hachmann, W.; Schaefer, M. M.; Seuffert, I.; Toensing, K.; Anselmetti, D. *Rev. Sci. Instrum.* **2008**, *79*, 063702.

(27) Sischka, A.; Eckel, R.; Toensing, K.; Ros, R.; Anselmetti, D. *Rev. Sci. Instrum.* **2003**, *74*, 4827−4831.

(28) Vandenplas, S.; Wiid, I.; Groblerrabie, A.; Brebner, K.; Ricketts, M.; Wallis, G.; Bester, A.; Boyd, C.; Mathew, C. *J. Med. Genet.* **1984**, *21*, 164−172.

(29) Antonin, W.; Riedel, D.; von Mollard, G. F. *J. Neurosci.* **2000**, *20*, 5724−5732.

(30) Skehan, P.; Storeng, R.; Scudiero, D.; Monks, A.; McMahon, J.; Vistica, D.; Warren, J. T.; Bokesch, H.; Kenney, S.; Boyd, M. R. *J. Natl. Cancer Inst.* **1990**, *82*, 1107−1112.

(31) Mammen, M.; Choi, S. K.; Whitesides, G. M. *Angew. Chem., Int. Ed.* **1998**, *37*, 2755−2794.

(32) Young, M. J.; Chin, J. *J. Am. Chem. Soc.* **1995**, *117*, 10577−10578.

(33) (a) Anbu, S.; Kandaswamy, M.; Varghese, B. *Dalton Trans.* **2010**, *39*, 3823−3832. (b) Zhang, Q.; Liu, J.; Chao, H.; Xue, G.; Li, L. *J. Inorg. Biochem.* **2001**, *83*, 49−55. (c) Wang, Y.; Xiao, W.; Mao, J. W.; Zhou, H.; Pan, Z. Q. *J. Mol. Struct.* **2013**, *1036*, 361−371. (d) Anbu, S.; Kandaswamy, M.; Suthakaran, P.; Murugan, V.; Varghese, B. *J. Inorg. Biochem.* **2009**, *103*, 401−410. (e) Arjmand, F.; Muddassir, M. *J. Photochem. Photobiol. B, Biol.* **2010**, *101*, 37−46.

(34) Tardito, S.; Bussolati, O.; Gaccioli, F.; Gatti, R.; Guizzardi, S.; Uggeri, J.; Marchio, L.; Lanfranchi, M.; Franchi-Gazzola, R. *Histochem. Cell Biol.* **2006**, *126*, 473−482.

(35) Glaser, T.; Liratzis, I.; Froehlich, R.; Weyhermueller, T. *Chem. Commun.* **2007**, 356−358.

(36) (a) Salata, M. R.; Marks, T. J. *J. Am. Chem. Soc.* **2008**, *130*, 12−13. (b) Rodriguez, B. A.; Delferro, M.; Marks, T. J. *J. Am. Chem. Soc.* **2009**, *131*, 5902−5919.

(37) (a) Becher, J.; Toftlund, H.; Olesen, P. H. *Chem. Commun.* **1983**, 740−742. (b) Anderson, O. P.; Becher, J.; Frydendahl, H.; Taylor, L. F.; Toftlund, H. *J. Chem. Soc., Chem. Commun.* **1986**, 699−701. (c) Bouwman, E.; Henderson, R. K.; Powell, A. K.; Reedijk, J.; Smeets, W. J. J.; Spek, A. L.; Veldman, N.; Wocadlo, S. *Dalton Trans.* **1998**, 3495−3499.

(38) (a) Li, H. J.; Crothers, D. M. *J. Mol. Biol.* **1969**, *39*, 461−477. (b) Schmechel, D. E.; Crothers, D. M. *Biopolymers* **1971**, *10*, 465−480. (c) Jennette, K. W.; Lippard, S. J.; Vassiliades, G. A.; Bauer, W. R. *Proc. Natl. Acad. Sci. U.S.A.* **1974**, *71*, 3839−3843. (d) Wolfe, A.; Shimer, G. H.; Meehan, T. *Biochemistry.* **1987**, *26*, 6392−6396. (e) Dougherty, G.; Pigram, W. J. *Crit. Rev. Biochem. Mol. Biol.* **1982**, *12*, 103−132.

(39) (a) Kotowycz, G. *Can. J. Chem.* **1974**, *52*, 924−929. (b) Eichhorn, G. L.; Clark, P.; Becker, E. D. *Biochemistry.* **1966**, *5*, 245−253. (c) Granot, J.; Feigon, J.; Kearns, D. R. *Biopolymers* **1982**, *21*, 181−201. (d) Banville, D. L.; Wilson, W. D.; Marzilli, L. G. *Inorg. Chem.* **1985**, *24*, 2479−2483.

(40) (a) Coury, J. E.; Anderson, J. R.; McFail-Isom, L.; Williams, L. D.; Bottomley, L. A. *J. Am. Chem. Soc.* **1997**, *119*, 3792−3796. (b) Arbuse, A.; Font, M.; Martínez, M. A.; Fontrodona, X.; Prieto, M. J.; Moreno, V.; Sala, X.; Llobet, A. *Inorg. Chem.* **2009**, *48*, 11098−11107. (c) Onoa, G. B.; Cervantes, G.; Moreno, V.; Prieto, M. J. *Nucleic Acids Res.* **1998**, *26*, 1473−1480. (d) Gamba, I.; Salvadó, I.; Rama, G.; Bertazzon, M.; Sánchez, M. I.; Sánchez-Pedregal, V. M.; Martínez-Costas, J.; Brissos, R. F.; Gamez, P.; Mascareñas, J. L.;

DOI: 10.1021/ic5028465
Inorg. Chem. 2015, 54, 2679−2690

Vázquez López, M.; Vázquez, M. E. *Chem.—Eur. J.* **2013**, *19*, 13369−13375.
(41) Heller, I.; Hoekstra, T. P.; King, G. A.; Peterman, E. J. G.; Wuite, G. J. L. *Chem. Rev.* **2014**, *114*, 3087−3119.
(42) King, G. A.; Gross, P.; Bockelmann, U.; Modesti, M.; Wuite, G. J. L.; Peterman, E. J. G. *Proc. Natl. Acad. Sci. U.S.A.* **2013**, *110*, 3859−3864.
(43) Rief, M. *Science* **1997**, *276*, 1109−1112.
(44) Bockelmann, U.; Thomen, P.; Essevaz-Roulet, B.; Viasnoff, V.; Heslot, F. *Biophys. J.* **2002**, *82*, 1537−1553.
(45) Strick, T.; Allemand, J.; Bensimon, D.; Croquette, V. *Biophys. J.* **1998**, *74*, 2016−2028.
(46) Strick, T. R.; Croquette, V.; Bensimon, D. *Nature* **2000**, *404*, 901−904.

DOI: 10.1021/ic5028465
Inorg. Chem. 2015, 54, 2679−2690